Spread Spectrum Time Domain Reflectometry with Lumped Elements on Asymmetric Transmission Lines

Ayobami S. Edun, *Student Member, IEEE,* Naveen Kumar Tumkur Jayakumar, *Student Member, IEEE,* Samuel Kingston[2], *Student Member, IEEE,* Cynthia Furse, *Fellow, IEEE,* Michael Scarpulla, *Member, IEEE,* Joel B. Harley, *Member, IEEE*

***Abstract*— Spread spectrum time domain reflectometry (SSTDR) has been traditionally used to detect hard faults (open and short circuit faults) in transmission lines. Prior work has focused on loads at the end of the line with little research on impedances from circuit elements located in the middle of the line (i.e., not at the load) or on only one wire of the line. In this work we consider cases of transmission lines with different impedances on each wire. We refer to lines with the same impedance on both wires (positive and negative) as symmetric. Lines with different impedances on each wire are asymmetric. For highly localized impedances (approximately infinitesimal in length, i.e. with a length significantly smaller than the wavelength of the incident signal), the reflections and their effects on the propagating wave become difficult to describe with traditional transmission line theory. We provide analytical expressions for reflection coefficients for symmetric and asymmetric transmission lines and show that these formulae describe experimental measurements of capacitors and resistors to about 99% accuracy for the magnitudes and 75% for the phases.**

***Index Terms*— Fault detection, impedance measurement, spread spectrum time domain reflectometry (SSTDR), transmission lines.**

I. Introduction and Motivation

TRANSMISSION lines are subject to numerous electrical faults that, if not quickly attended to, can result in electrical fires, increased system downtime, and reduced system efficiency [1], [2]. Transmission lines are also susceptible to line-to-ground faults, line-to-line faults, and three phase faults [3]. These faults constitute impedance variations on the line, can occur anywhere along the transmission line, and are often highly localized. Similarly, faults can occur where transmission lines connect to local devices, such as photovoltaics (PV). In this paper, we analyze impedance changes that are highly localized and act effectively as lumped elements. These lumped elements can be symmetrically placed in parallel or in series on both wires of the transmission line or asymmetrically placed on only one wire of the transmission line.

Prior work has demonstrated that reflectometry can accurately locate open circuit faults and short circuits in transmission lines [4]. In these schemes, an incident signal is sent through the electrical system. This signal reflects at points of impedance mismatch [5] and returns to the transmitting point, where it is measured. The time delay between the incident and reflected signals gives the distance to the fault [6] while the amplitude and phase of the reflection gives the strength and characteristics of the impedance mismatch [7].
There are several types of reflectometry [4]. We will use Spread spectrum time domain reflectometry (SSTDR) [6], [8] for the assessment in this paper, however the results are applicable to all other types of reflectometry as well. In this paper, we will demonstrate the accuracy of our evaluation methods by using spread spectrum time domain reflectometry (SSTDR), which uses a modulated pseudo-noise (PN) code as the test signal [8], [9]. The theory we develop in this paper applies to other forms of reflectometry as well.

Most prior work using reflectometry techniques considers either reflections from loads (impedances) at the end of the transmission line (e.g., parallel open or short circuits) or impedances distributed uniformly along the length of the transmission line (e.g., for the analysis of soil moisture [10]). Note that open or short circuit faults in the middle of a line effectively create the end of the line at their location, and signals cannot propagate past them. Smaller impedance discontinuities that are short enough in length that they effectively act like a lumped element (e.g., from a resistive or capacitive sensor, a solar cell, or other circuit element) in the middle of a transmission line have been analyzed [11]. These analyses show the potential for reflectometry to locate and measure complex impedances embedded along the length of

This material is based upon work supported by the U.S. Department of Energy's Office of Energy Efficiency and Renewable Energy (EERE) under Solar Energy Technologies Office (SETO) Agreement Number DE-EE0008169. Also, we want to express gratitude to Gardner Energy (West Haven, UT) for their support with testing on their PV modules.
Ayobami Edun is with Department of Electrical and Computer Engineering, University of Florida, Gainesville, FL 32611 USA (e-mail: aedun@ufl.edu)
Naveen Kumar Tumkur Jayakumar was with Department of Electrical and Computer Engineering, University of Utah, Salt Lake City, UT 84112 USA (e-mail: naveentj92@gmail.com).
Samuel Kingston is with Department of Electrical and Computer Engineering University of Utah, Salt Lake City, UT 84112 USA (e-mail: u0763921@utah.edu).
C. Furse is with the Department of Electrical and Computer Engineering, University of Utah, Salt Lake City, UT 84112 USA, and with the LiveWire Test Labs, Inc., Salt Lake City, UT 84117 USA (e-mail: cfurse@ece.utah.edu).
Michael Scarpulla is with Department of Electrical and Computer Engineering University of Utah, Salt Lake City, UT 84112 USA (e-mail: mike.scarpulla@utah.edu).
Joel B. Harley is with Department of Electrical and Computer Engineering, University of Florida, Gainesville, FL 32611 USA (e-mail: joel.harley@ufl.edu)

transmission lines. Small faults such as chafes and frays have also been analyzed [12]–[14]. These are notoriously difficult to detect and locate, because the reflections they produce are very small (due to small changes in impedance), and the reflection at the start of the fault overlaps and nearly negates the reflection from the end of the fault, due to their short length. Our analysis methods apply to these types of faults as well.

In this paper, we evaluate lumped elements (resistors and capacitors) in a series (ring) connection and parallel (ladder) connection. This is in preparation for finding faults in photovoltaic (PV) arrays, where each PV module presents a complex impedance. We will consider impedances on only one wire (positive/negative) of a two-wire line (typical of a PV installation), creating an asymmetric system. In section 2 of this paper, we investigate and model very short impedance discontinuities (such as lumped elements) in both symmetric and asymmetric transmission lines, such as found in photovoltaic strings while also extending the study to a parallel impedance case. Modified reflection and transmission coefficients are introduced to account for effectively infinitesimally short impedances along transmission lines.

To validate these theoretical derivations, section 3 describes SSTDR experiments with (lumped element) resistors and capacitors in symmetric and asymmetric transmission line configurations. In our experiments, we convert the time domain SSTDR reflectometry response to the frequency domain to measure the magnitude and phase of the reflection coefficients as a function of frequency for each of these setups. Our results show an excellent match with a minimum confidence level of greater than 99% between our theory and the experimental data. In addition, we will discuss how our results infer strategies for identifying and locating faults for both symmetric and asymmetric transmission lines. Conclusions and future work are discussed in section 4.

II. Modeling Infinitesimally Short Impedance Discontinuities in Transmission Lines.

A. Transmission Line Model and Reflection Coefficient in the Frequency Domain

A transmission line connects a source on one end to a load at the other end as shown in Fig. 1. Two wires make up the transmission line, connected to + and – terminals. When an incident signal (V_{inc}) is sent down the line, it reflects at Z_L, producing a reflected voltage (V_{ref}) that returns to the test end and can be measured there. This reflection is described by the complex frequency domain reflection coefficient at the load:

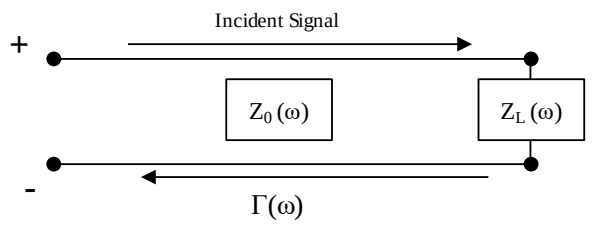

Fig. 1. Transmission line with a load.

$$\Gamma(\omega) = \frac{V_{ref}}{V_{inc}} = \frac{Z_L(\omega) - Z_o(\omega)}{Z_L(\omega) + Z_o(\omega)} \quad (1)$$

where $Z_0(\omega)$ is the line's characteristic impedance, and $Z_L(\omega)$ is the load impedance. When the end of the line is an open circuit, we expect a complete reflection with a reflection coefficient of 1, and a short circuit gives a reflection coefficient of -1. Most prior work has focused on locating shorts and opens at the end of the transmission line. This paper studies the reflection behavior of arbitrary real and complex impedances anywhere along the transmission line.

Traditionally, a discontinuity in the middle of the line can be modelled as part of a multi-segment transmission line, shown in Fig. 2. This Figure illustrates three transmission lines with characteristics impedances $Z_{01}(\omega)$, $Z_i(\omega)$, and $Z_{02}(\omega)$. We refer to the middle line as an interface between transmission lines 1 and 2. The reflection and transmission coefficient in each segment can be defined using the systematic solution procedure by [15]:

$$\Gamma_2(z=0) = \frac{Z_{02}(\omega) - Z_i(\omega)}{Z_{02}(\omega) + Z_i(\omega)} \quad (2)$$

$$T_2(\omega) = 1 + \Gamma_2(\omega) = \frac{2Z_{02}(\omega)}{Z_i(\omega) + Z_{02}(\omega)} \quad (3)$$

$$\Gamma_2(z=-l) = \Gamma_2(0)e^{2\beta(-l)} \quad (4)$$

$$Z^{total}(z=-l) = Z_i(\omega)\left(\frac{1+\Gamma_2(-l)}{1-\Gamma_2(-l)}\right) \quad (5)$$

$$\Gamma_1(\omega) = \frac{Z^{total}(-l) - Z_{01}(\omega)}{Z^{total}(-l) + Z_{01}(\omega)} \quad (6)$$

When the interface transmission line's length is negligibly small (as for a lumped element), i.e., $l \approx 0$, the reflection coefficient at each boundary can be defined by

$$\Gamma_2(z=-l) = \Gamma_2(0)e^{2\beta(-0)} = \Gamma_2(0) \quad (7)$$

$$Z^{total}(z=-l) = Z_i(\omega)\left(\frac{1+\Gamma 2(0)}{1-\Gamma 2(0)}\right) \quad (8)$$

$$Z^{total}(z=-l) = Z_i(\omega)\left(\frac{2Z_{02}(\omega)}{\frac{Z_i(\omega)+Z_{02}(\omega)}{2Z_i(\omega)}}{Z_i(\omega)+Z_{02}(\omega)}\right) = Z_{02}(\omega) \quad (9)$$

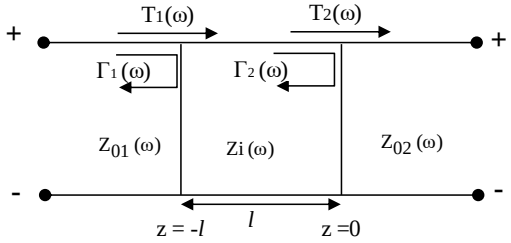

Fig. 2: Transmission line with impedance at the middle of the line with the reflection and transmission coefficients.

$$\Gamma_1(\omega) = \frac{Z^{total}(-l) - Z_{01}(\omega)}{Z^{total}(-l) + Z_{01}(\omega)} = \frac{Z_{02}(\omega) - Z_{01}(\omega)}{Z_{02}(\omega) + Z_{01}(\omega)} \quad (10)$$

Where β is phase constant, $\Gamma_1(\omega)$ is the reflection coefficient at the front of the interface and $\Gamma_2(\omega)$ is the reflection coefficient at the end of the interface. Hence, when the length of the interface is infinitesimally small, and the transmission line segments before and after the interface are equal, the total reflection coefficient observed at the front of the interface is 0. This derivation illustrates that traditional theory cannot be used to analyze lumped elements (near-zero-length impedance changes) in a transmission line.

This approach works well to analyze systems defined by characteristic impedances, but it does not accurately represent what happens if we have a lumped element (e.g., a resistor, capacitor, PV module, or other circuit element) in the system. This lumped element is fundamentally different than the transmission line interface segment above. When we consider the characteristic impedance of a transmission line, this represents a ratio of voltage and current travelling in only one direction (forward or backward). When we consider the lumped element impedance, it represents the ratio of the total voltage and current, which are a combination of the incident (positive-traveling) and reflected (negative-traveling) voltages and currents. Thus, we handle this lumped element impedance in a fundamentally different way than we handle the transmission line impedance above. Notably, in all these cases, characteristic impedance $Z_{02}(\omega)$ represents both the characteristic and total impedance at that location since there are no reflections on this infinitely long line. In the next section, we will re-derive reflections at lumped impedances.

B. Reflection and Transmission Coefficient for a Spatially Small Impedance in an Asymmetric line

In this section, we consider the reflection coefficient from a lumped impedance that is effectively infinitesimally small in length, as shown in Fig. 3a. The lumped element is placed on only one of the two wires that make up the transmission line, thus creating an asymmetric system. We refer to this infinitesimally small impedance as an interface impedance, since it is found between two points (*A* and *B)* of the transmission line. To generalize our theory, we assume the transmission line has different characteristic impedances before $Z_{01}(\omega)$ and after $Z_{02}(\omega)$ the interface impedance.

We determine the reflection coefficient at the interface in a manner similar to analysis of power splitting in microwave circuits [16]. Specifically, we assume the interface is located at point z=0 The characteristic impedance after the interface ($Z_{02}(\omega)$) is modeled as a load between points A and B, as shown in Fig. 3(b). An equivalent load impedance $Z_L(\omega)$ is found by summing $Z_{02}(\omega)$ with the interface impedance $Z_L(\omega) = Z_{02}(\omega) + Z_{i\ asym}(\omega)$. Plugging this effective load impedance into (1), the complex, frequency-domain reflection coefficient at the interface is defined by

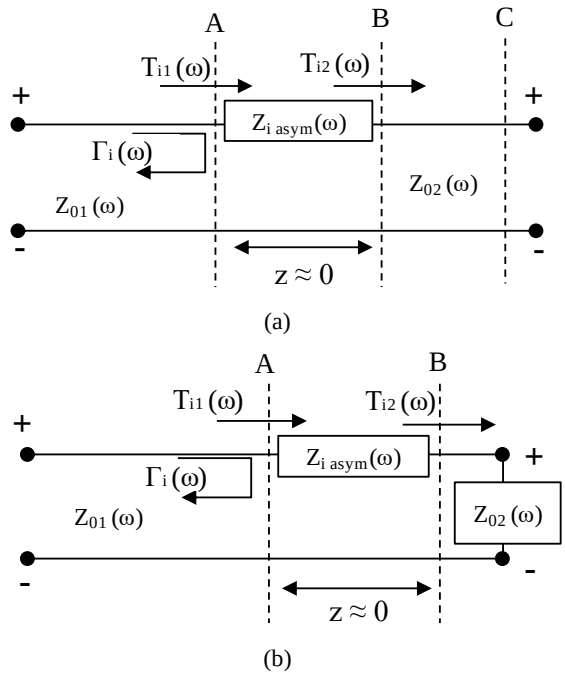

Fig. 3. A lumped impedance (Zi) attached between two transmission lines, where the second transmission line is (a) An infinitely long transmission line and (b) the equivalent circuit of the infinitely long line.

$$\Gamma i(\omega) = \frac{Z_L(\omega) - Z_{01}(\omega)}{Z_L(\omega) + Z_{01}(\omega)} = \frac{Z_{iasym}(\omega) + Z_{02}(\omega) - Z_{01}(\omega)}{Z_{iasym}(\omega) + Z_{02}(\omega) + Z_{01}(\omega)} \quad (11)$$

The corresponding transmission coefficient from the interface to the layer between *B* and *C* is defined as:

$$T_{i1}(\omega) = 1 + \Gamma i(\omega) = \frac{2(Z_{iasym}(\omega) + Z_{02}(\omega))}{Z_{iasym}(\omega) + Z_{02}(\omega) + Z_{01}(\omega)} \quad (12)$$

Considering a voltage divider, $T_{i2}(\omega)$ is:

$$T_{i2}(\omega) = \frac{Z_{02}(\omega)}{Z_{iasym}(\omega) + Z_{02}(\omega)} T_{i1}(\omega) \quad (13)$$

$$T_{i2}(\omega) = \frac{2Z_{02}(\omega)}{Z_{iasym}(\omega) + Z_{02}(\omega) + Z_{01}(\omega)} \quad (14)$$

When the two transmission line segments have the same characteristic impedances (i.e., $Z_{01}(\omega) = Z_{02}(\omega) = Z_0(\omega)$) the coefficient simplifies to

$$\Gamma i(\omega) = \frac{Z_{iasym}(\omega)/2}{Z_{isym}(\omega)/2 + Z_0(\omega)} \quad (15)$$

$$Ti(\omega) = \frac{Z_0(\omega)}{Z_{iasym}(\omega)/2 + Z_0(\omega)} \quad (16)$$

These expressions correspond to a voltage divider in circuit theory between half of $Z_{i\ asym}(\omega)$ and $Z_o(\omega)$. Note that when the interface impedance $Z_{i\ asym}(\omega) = 0$, a series short circuit, the reflection coefficient from the interface will be 0 and the

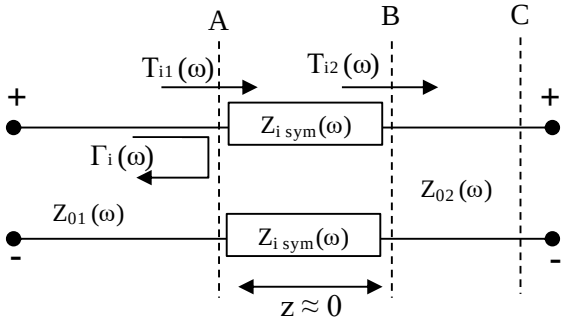

Fig. 4. Infinitesimally small impedance on symmetric line

transmission coefficient will be 1, as expected. Also note that for most practical transmission lines, the characteristic impedances vary only minimally with frequency.

C. Reflection and Transmission Coefficient for a Spatially Small Impedance in a Symmetric Line

The line is symmetric when two equal lumped impedances ($Z_{isym}(\omega)$) are at the same location on both wires of the line, as in Fig. 4. Using the same approach as in the previous section, the complex, frequency-domain reflection coefficient at the interface is

$$\Gamma_i(\omega) = \frac{2Z_{isym}(\omega) + Z_{02}(\omega) - Z_{01}(\omega)}{2Z_{isym}(\omega) + Z_{02}(\omega) + Z_{01}(\omega)} \quad (17)$$

Note that this implies that when the interface impedances of a symmetric line are half that of the interface impedance of the asymmetric line, we expect to observe the same reflections. This also implies that, in the symmetric configuration, the interface impedances act as if they are in series.

Similarly, we define a transmission coefficient from the interface of the spatially small impedance as:

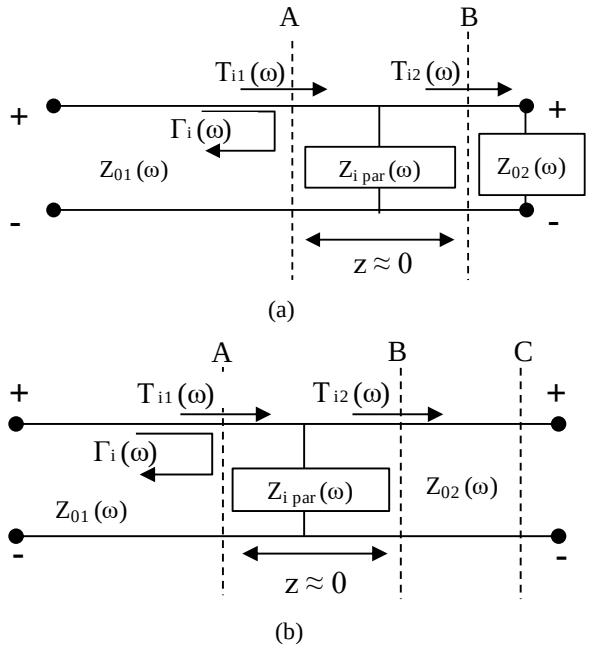

Fig. 5. (a) Infinitesimally small impedance for parallel impedance between the line. (b) Equivalent circuit.

$$T_{i1}(\omega) = 1 + \Gamma_i(\omega) = \frac{2(2Z_{isym}(\omega) + Z_{02}(\omega))}{2Z_{isym}(\omega) + Z_{02}(\omega) + Z_{01}(\omega)} \quad (18)$$

$T_{i2}(\omega)$ then becomes:

$$T_{i2}(\omega) = \frac{Z_{02}(\omega)}{Z_{iasym}(\omega) + Z_{02}(\omega)} T_{i1}(\omega) \quad (19)$$

$$T_{i2}(\omega) = \frac{2Z_{02}(\omega)}{2Z_{isym}(\omega) + Z_{02}(\omega) + Z_{01}(\omega)} \quad (20)$$

When the characteristic impedances on both wires of the interface are equal (i.e., $Z_{01}(\omega) = Z_0(\omega) = Z_{02}(\omega)$), the reflection and transmission coefficients of a symmetric line simplifies to a voltage divider between $Z_{i\,sym}(\omega)$ and $Z_0(\omega)$:

$$\Gamma_i(\omega) = \frac{Z_{isym}(\omega)}{Z_{isym}(\omega) + Z_0(\omega)} \quad (21)$$

$$T_i(\omega) = \frac{Z_0(\omega)}{Z_{isym}(\omega) + Z_0(\omega)} \quad (22)$$

D. Reflection and Transmission Coefficient for a Spatially Small Impedance in Parallel to the Line

We extend our theoretical derivation to the case where there is a parallel impedance across the transmission line, as shown in Fig. 5. Using the same theoretical technique as in the series case, we assume the transmission line has different characteristic impedances before ($Z_{01}(\omega)$) and after ($Z_{02}(\omega)$) a parallel impedance $Z_{ipar}(\omega)$. In the equivalent circuit, the load impedance $Z_L(\omega)$ becomes $Z_{ipar}(\omega) \parallel Z_{02}(\omega)$. The reflection coefficient can then be found using (1):

$$\Gamma_i(\omega) = \frac{Z_{02}(\omega) + \dfrac{Z_{01}(\omega)Z_{01}(\omega)}{Z_{ipar}(\omega)} - Z_{01}(\omega)}{Z_{02}(\omega) + \dfrac{Z_{01}(\omega)Z_{01}(\omega)}{Z_{ipar}(\omega)} + Z_{01}(\omega)} \quad (23)$$

Note that when $Z_{ipar}(\omega) = 0$, a short, the reflection coefficient is -1 and when $Z_{ipar}(\omega) = \infty$, an open, then we get a reflection coefficient of:

$$\Gamma_i(\omega) = \frac{Z_{02}(\omega) - Z_{01}(\omega)}{Z_{02}(\omega) + Z_{01}(\omega)} \quad (24)$$

When $Z_{01}(\omega) = Z_0(\omega) = Z_{02}(\omega)$, the reflection coefficient at the interface becomes:

$$\Gamma_i(\omega) = \frac{-Z_0(\omega)}{2Z_{ipar}(\omega) + Z_0(\omega)} \quad (25)$$

Since voltages in parallel are equal, $T_{i1}(\omega) = T_{i2}(\omega)$,

$$T_i(\omega) = 1 + \Gamma_i(\omega) = \frac{2Z_{ipar}(\omega)}{2Z_{ipar}(\omega) + Z_0(\omega)} \quad (26)$$

III. Comparison with Measurements

To test the theoretical reflection coefficients, we used spread spectrum time domain reflectometry (SSTDR) [11] to transmit a 24MHz square wave modulated pseudo noise (PN) signal into a transmission line and then measure and analyze its

reflections. For our experiments, we used a WILMA W50A000F SSTDR (from Livewire Innovation) [17]. The incident signal is sent down the transmission line where it reflects at points of impedance mismatch. The reflected signal is then correlated in the SSTDR device with a delayed version of the incident signal to produce the reflectometry signature. To calculate the distance, the sample time is multiplied by the velocity of propagation to convert it to distance.

The twin lead cable was made up of 10 AWG multi-conductor cross-linked polyethylene (XLPE) coated 2000 V photovoltaic PV wires [18] taped together to form a twin-lead cable. The cable has a characteristic impedance of 178Ω. Other parameters of this twin-lead cable are given in Table I. [19]. We measured the reflection coefficients for parallel interface impedances as shown in Fig. 6 and for serial interface impedances as shown in Fig. 7. The variables $Z_{iA}(\omega)$, $Z_{iB}(\omega)$, and $Z_{ipar}(\omega)$ represent lumped impedances that can be plugged into specialized connectors that allow us to attach resistors, capacitors, etc. in series or parallel with the twin lead transmission line [19].

For the series case (Fig. 7), we consider either a symmetric or asymmetric system. The symmetric system has $Z_{iA}(\omega) = Z_{iB}(\omega)$ (resistors or capacitors in our tests), and the end of the line is open. The asymmetric setup has $Z_{iA}(\omega)$ or $Z_{iB}(\omega)$ equal to zero (a short circuit/wire), and the end of the line is open. The parallel setup (Fig. 6) also has $Z_{ipar}(\omega)$ for resistor and capacitor values while the end of the line is also open.

When a signal is sent down the line, there are reflections from where the SSTDR connects to the transmission line and from the connectors in the system. We can remove these reflections from our analysis by using a baseline measurement of the basic system (with $Z_{iA}(\omega) = Z_{iB}(\omega) = 0$ in Fig. 7). The baseline will be subtracted from all other measured data to remove the reflections from connectors, etc.

Resistors and ceramic capacitors were used for $Z_{iA}(\omega)$, $Z_{iB}(\omega)$, and $Z_{ipar}(\omega)$. We considered resistor values of 10, 20, 30, 56, 130, 503, 1000, 2000 Ω and capacitor values of 470, 330, 100, 47, 25, 20, 15, 8, 5, 2, 1 pF.

Fig. 8a shows the time domain reflection signature of our baseline, an asymmetric system with $Z_{iA}(\omega) = 20\Omega$ or $Z_{iB}(\omega)$ = 20pF. Each reflection signature was normalized by its maximum value. The reflection at 0m is from the change in impedance between the SSTDR and the line. The next reflection is from $Z_i(\omega)$. The final reflection is from the open circuit at the end of the line. For each measurement, we subtract the baseline from the reflection yielding, for example, the signature shown in Fig. 8b for the case where $Z_{iA}(\omega) = 20\Omega$. We then isolate (time-gate) the reflection at $Z_i(\omega)$, assuming the line after the interface is sufficiently long that additional reflections do not overlap with the reflection from the interface. The baseline subtracted reflection signature is shown in Fig. 8b, and the extracted reflection signatures for capacitors and resistors are shown in Fig. 9 and Fig. 10 respectively.

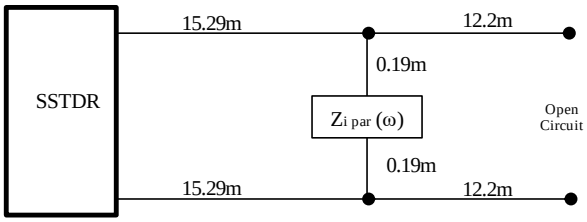

Fig. 6: Experimental Setup for the parallel impedance.

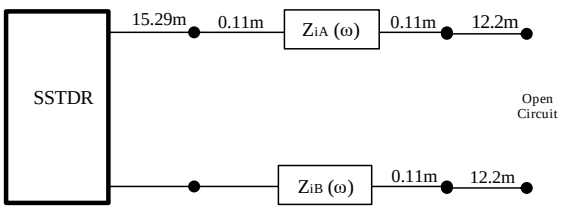

Fig. 7. Experimental Setup for the series impedance.

Table I
PV cable and SSTDR parameters

Parameters	Values
Conductor diameter (d_c)	2.94 mm
Conductivity of copper (σ_c)	5.98×10^7 S/m
Loss tangent of XLPE	4×10^{-4}
μ_{rXLPE}	0.999994
XLPE insulation thickness (t_{in})	3.375 mm
Distance between conductors (D_c)	11 mm
ε_{rXLPE}	2.3
Z_{SSTDR}	68 Ω
f_m	24 MHz
v_o *(times speed of light)*	0.722 ± 0.008
Z_o	178 Ω
Z_{SSTDR}	68 Ω

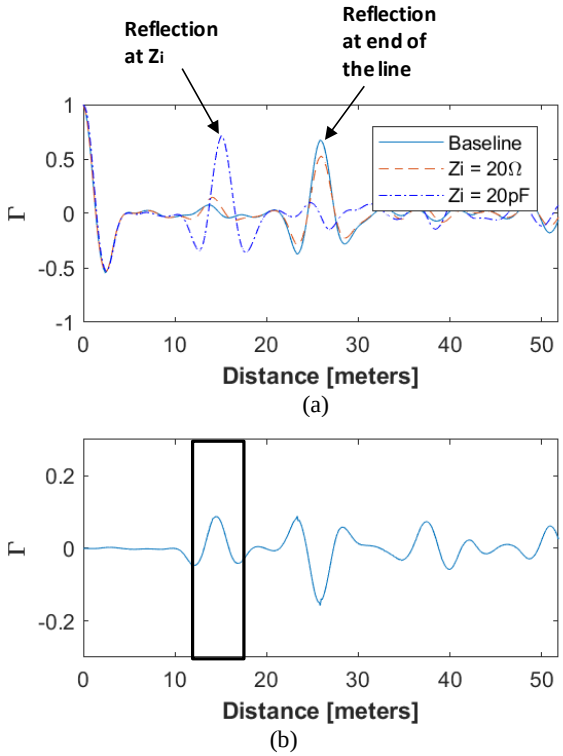

Fig. 8. a) time domain reflection signature for baseline, 20 ohms resistor and 20pF capacitor. b) Time-gating the first reflection of a baseline subtracted reflection signature for $Z_{iA}(\omega) = 20\Omega$.

A. Time-domain Reflection signatures

Fig. 9 shows the measured time-domain baseline subtracted reflection signatures for resistances. Reflections from series interface impedances (shown in Fig. 7) are shown for both symmetric cases (Fig. 9a) and asymmetric cases (Fig. 9b). We see that the magnitude of the reflection coefficient increases as the resistor values increase. Reflections from parallel interface impedances (shown in Fig. 6) are shown in Fig. 9c. The magnitude of the reflection decreases as the resistor values increase. For all resistances (series and parallel), the shape of the reflection is symmetric with time. Reflections from resistors have the same shape as for an open circuit, but a lower magnitude. Fig. 10 shows the measured time-domain baseline subtracted reflection signatures for capacitances. Reflections from series interface impedances (shown in Fig. 7) are shown for both symmetric cases (Fig. 10a) and asymmetric cases (Fig. 10b). Reflections from parallel interface impedances (shown in Fig. 6) are shown in Fig. 10c. For capacitors, the shape of the waveform changes significantly. This is because their impedance ($1/j\omega C$) is frequency-dependent, which creates frequency dispersion in the time domain reflection.

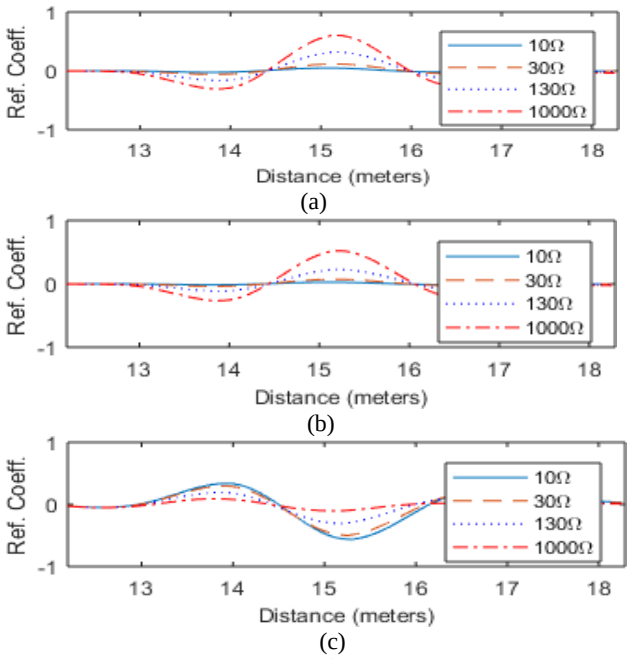

Fig. 9. SSTDR time-domain reflections (baseline subtracted reflection signatures) for the first interface reflection for resistors that are a) Symmetric in series, b) Asymmetric in series, c) Parallel.

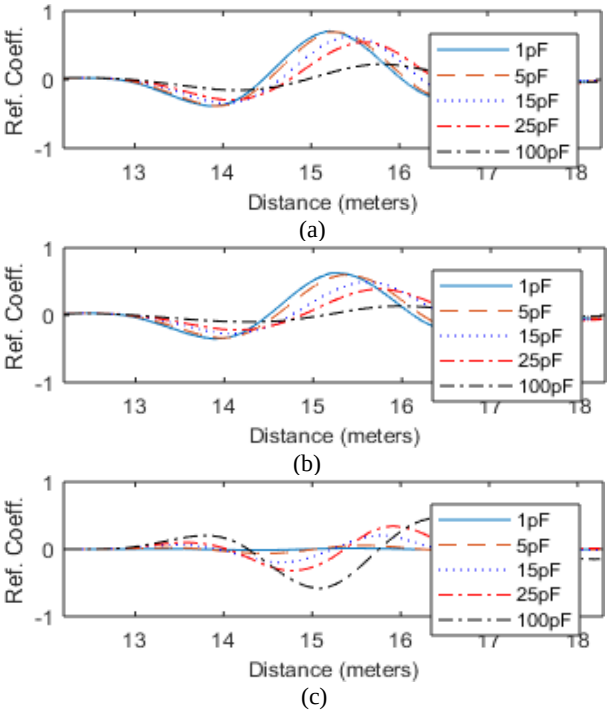

Fig. 10. SSTDR time-domain reflections (baseline subtracted reflection signatures) for the first interface reflection for capacitors that are a) Symmetric in series, b) Asymmetric in series, c) Parallel.

B. Reflection Coefficients

From the time-domain reflection coefficients in Fig. 9 and Fig. 10, we compute the fast Fourier transform, which gives the reflection coefficient as a function of frequency. There are 15 samples (Δt =10.42 ms) in the time-gated reflection signature (Fig. 9 and Fig. 10). To increase the frequency resolution of the FFT, we zero pad the end of the time gated signal to 40,960 points and Δf = 4.68 kHz. From the FFT, we extract the magnitude and phase of the reflection coefficient at 24 MHz (the modulation frequency of our SSTDR) and compare this measured reflection coefficient to the theoretical reflection coefficients derived in Section 2.

Fig. 11 shows the magnitude and phase of the reflection coefficient for a symmetric series interface impedance (i.e., the same impedance value on both wires of the transmission line, as shown in Fig. 4) for a range of resistive interface impedances. Fig. 12 shows the reflection coefficients for symmetric series capacitors. The solid line represents the

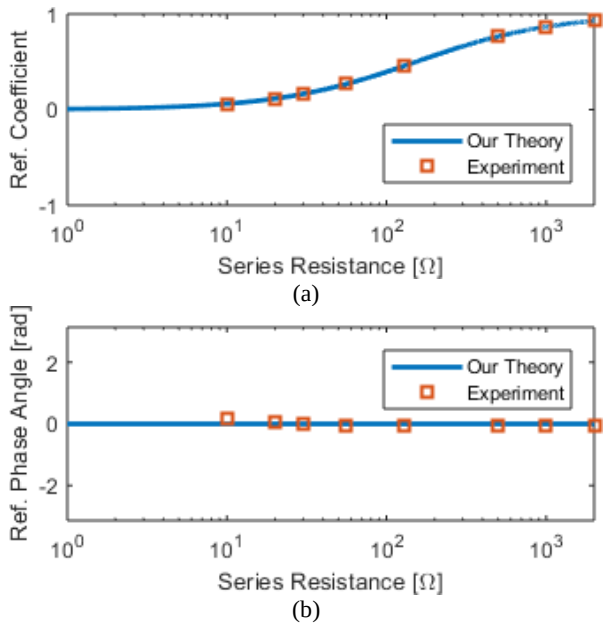

Fig. 11. (a) Magnitude and (b) phase of the reflection coefficient for the theoretical (from (21)) and measured data for symmetric resistors

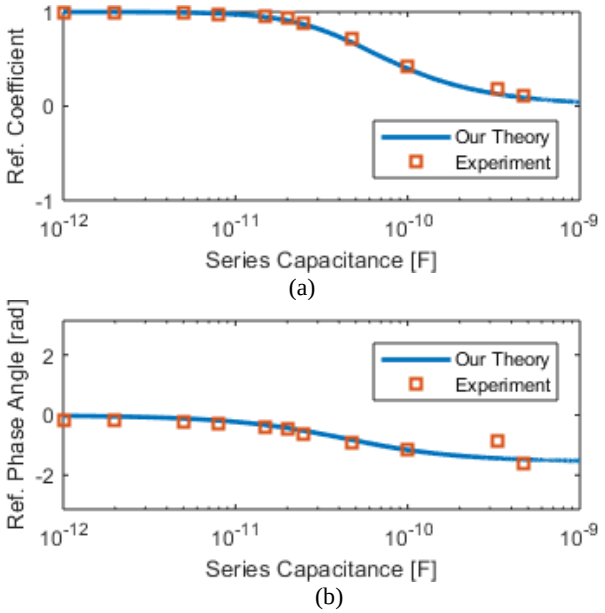

Fig. 12. (a) Magnitude and (b) phase of the reflection coefficient for the theoretical (from (21)) and measured data for symmetric capacitors

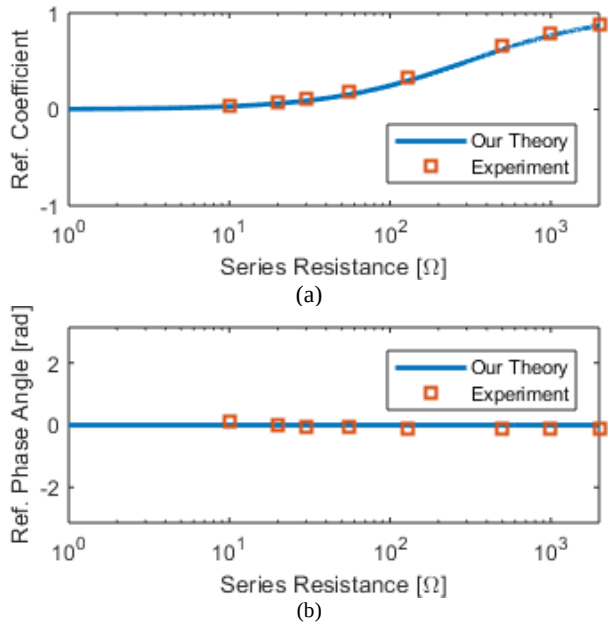

Fig. 13. (a) Magnitude and (b) phase of the reflection coefficient for the theoretical (from (15)) and measured data for asymmetric resistors.

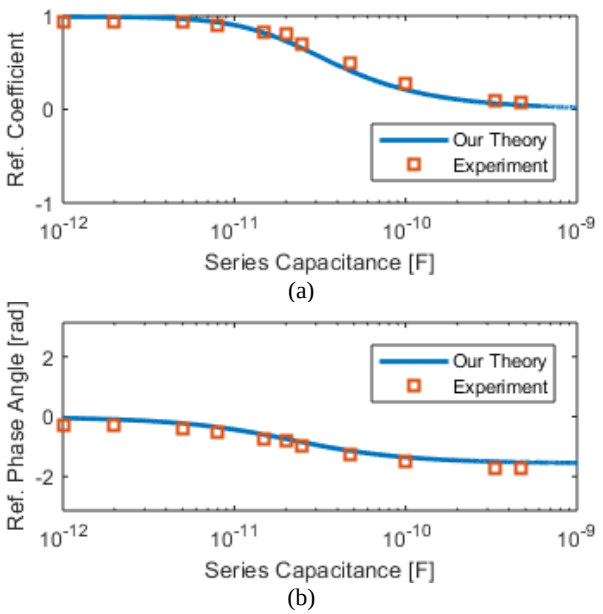

Fig. 14. (a) Magnitude and (b) phase of the reflection coefficient for the theoretical (from (15)) and measured data for asymmetric capacitors

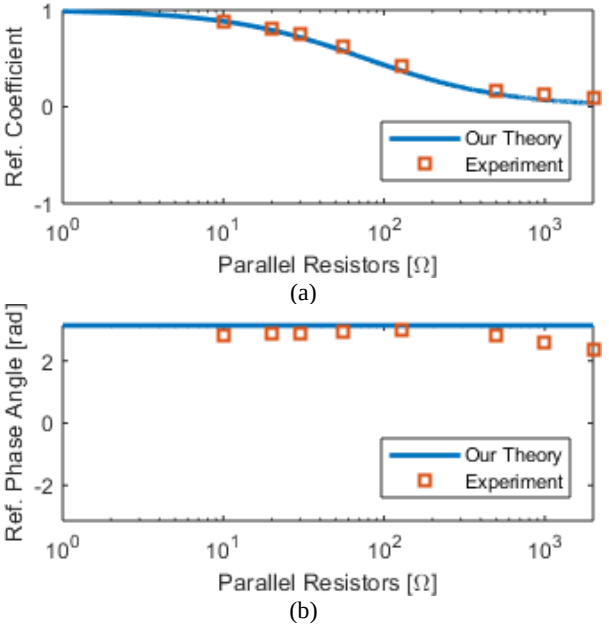

Fig. 15. (a) Magnitude and (b) phase of the reflection coefficient for the theoretical (from ((25)) and measured data for parallel resistors.

theoretical results (from equation (21)), and the square points represent the measurements.

Excellent agreement between theoretical and measured reflection coefficients is seen. For asymmetric series interface impedances (i.e., the impedance on one wire of the transmission line, as shown in Fig. 3), Fig. 13 and Fig. 14 show the reflection coefficients after placing a resistor (Fig. 13) or capacitor (Fig. 14) in $Z_{iB}(\omega)$ only. The measured reflection coefficients show excellent agreement with the theoretical reflection coefficient in (15).

For parallel interface impedances (Fig. 6), Fig. 15 and Fig. 16 show the reflection coefficients after placing a resistor (Fig. 14) or capacitor (Fig. 16) in $Z_{ipar}(\omega)$. The measured reflection coefficients show excellent agreement with the theoretical reflection coefficient in (25)).

IV. Conclusions and Future Work

Spread spectrum time domain reflectometry is a viable means of locating faults on energized transmission lines. To properly interpret the results from SSTDR, the underlying principles must be understood. This work has extended SSTDR analysis to cases where there are infinitesimally long

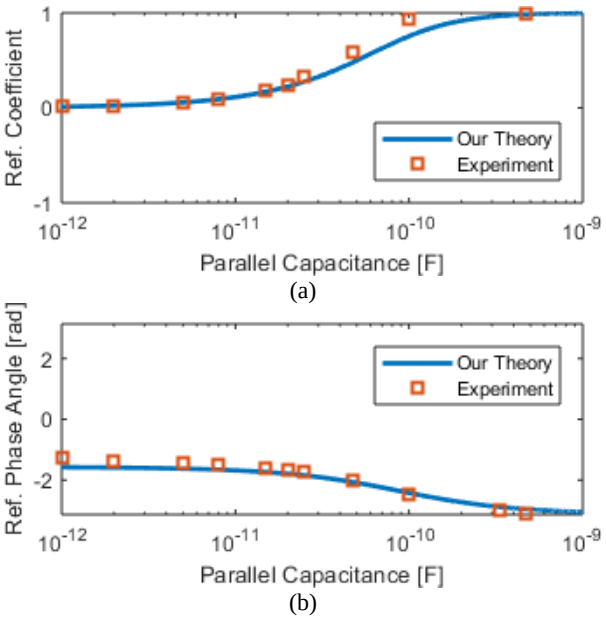

Fig. 16. (a) Magnitude and (b) phase of the reflection coefficient for the theoretical (from ((25)) and measured data for Parallel capacitors.

impedances and asymmetric transmission lines by deriving new reflection coefficients.

Our theory was compared with experiments, and results show a near perfect match. For each setup, we correlated the magnitude of the reflection coefficient obtained from experiment with the theoretical result. This gives a 99% match for the symmetric, asymmetric and parallel setups for both resistor and capacitor values. A similar comparison for phase shows a 71% match for asymmetric resistor, 99% for asymmetric capacitors, 75% for symmetric resistors, 92% for symmetric capacitors, 99% match for parallel capacitors and 65% for parallel resistors. Discrepancy in the results could be attributed to parasitic inductance, resistance and capacitance in real-world elements. Such parasitic parameters are also frequency dependent. These results could be extended to many applications, such as the evaluation of sensors or photovoltaic panels connected by transmission lines. Future work will study multiple reflection behavior, particularly with respect to detecting faults in photovoltaic modules connected via transmission lines.

V. Disclosure

Dr. C.M. Furse is a co-founder of LiveWire Innovation, Inc. which is commercializing SSTDR technology, and therefore has a financial conflict of interest with this company.

VI. References

[1] M. K. Alam, F. Khan, J. Johnson, and J. Flicker, "A Comprehensive Review of Catastrophic Faults in PV Arrays: Types, Detection, and Mitigation Techniques," *IEEE J. Photovolt.*, vol. 5, no. 3, pp. 982–997, May 2015.

[2] S. Chen, X. Li, Z. Xie, and Y. Meng, "Time–Frequency Distribution Characteristic and Model Simulation of Photovoltaic Series Arc Fault with Power Electronic Equipment," *IEEE J. Photovolt.*, vol. 9, no. 4, pp. 1128–1137, Jul. 2019.

[3] H. Choi, Y. Cho, B. Jung, D. Chung, and A. Fathy, "Comparison of the Unbalanced Faults in Three-Phase Resistive and Matrix-Type SFCLs," *IEEE Trans. Appl. Supercond.*, vol. 20, no. 3, pp. 1215–1218, Jun. 2010.

[4] C. Furse, Y. C. Chung, C. Lo, and P. Pendayala, "A critical comparison of reflectometry methods for location of wiring faults," *Smart Struct. Syst.*, vol. 2, no. 1, pp. 25–46, 2006.

[5] C. Furse, You Chung Chung, R. Dangol, M. Nielsen, G. Mabey, and R. Woodward, "Frequency-domain reflectometry for on-board testing of aging aircraft wiring," *IEEE Trans. Electromagn. Compat.*, vol. 45, no. 2, pp. 306–315, May 2003.

[6] C. Furse, P. Smith, C. Lo, Y. C. Chung, P. Pendayala, and K. Nagoti, "Spread spectrum sensors for critical fault location on live wire networks," *Struct. Control Health Monit.*, vol. 12, no. 3–4, pp. 257–267, 2005.

[7] C. Furse *et al.*, "Spread Spectrum Time Domain Reflectometry for Complex Impedances: Application to PV Arrays," in *2018 IEEE AUTOTESTCON*, 2018, pp. 1–4.

[8] Zha Wenqi, Wang Li, and Chen Wei, "Theoretical and experimental study of Spread Spectral Domain Reflectometry," in *Railway and Ship Propulsion 2012 Electrical Systems for Aircraft*, 2012, pp. 1–5.

[9] C. Furse, P. Smith, C. Lo, Y. C. Chung, P. Pendayala, and K. Nagoti, "Spread spectrum sensors for critical fault location on live wire networks," *Struct. Control Health Monit.*, vol. 12, no. 3–4, pp. 257–267, 2005.

[10] W. Sheng *et al.*, "A TDR array probe for monitoring near-surface soil moisture distribution," *Vadose Zone J.*, vol. 16, no. 4, Apr. 2017.

[11] M. U. Saleh *et al.*, "Signal Propagation Through Piecewise Transmission Lines for Interpretation of Reflectometry in Photovoltaic Systems," *IEEE J. Photovolt.*, vol. 9, no. 2, pp. 506–512, Mar. 2019.

[12] S. Schuet, D. Timucin, and K. Wheeler, "A Model-Based Probabilistic Inversion Framework for Characterizing Wire Fault Detection Using TDR," *IEEE Trans. Instrum. Meas.*, vol. 60, no. 5, pp. 1654–1663, May 2011.

[13] L. A. Griffiths, R. Parakh, C. Furse, and B. Baker, "The invisible fray: a critical analysis of the use of reflectometry for fray location," *IEEE Sens. J.*, vol. 6, no. 3, pp. 697–706, Jun. 2006.

[14] E. J. Lundquist, J. R. Nagel, S. Wu, B. Jones, and C. Furse, "Advanced Forward Methods for Complex Wire Fault Modeling," *IEEE Sens. J.*, vol. 13, no. 4, pp. 1172–1179, Apr. 2013.

[15] "Waveland Press - Electromagnetic Fields and Waves, Second Edition, by Magdy F. Iskander." [Online]. Available: http://www.waveland.com/browse.php?t=389. [Accessed: 16-Oct-2019].

[16] S. W. Wong and L. Zhu, "Ultra-Wideband Power Divider with Good In-Band Splitting and Isolation Performances," *IEEE Microw. Wirel. Compon. Lett.*, vol. 18, no. 8, pp. 518–520, Aug. 2008.

[17] "Live Cable Fault Detection by LiveWire Innovation." [Online]. Available: https://www.livewireinnovation.com/. [Accessed: 02-Oct-2019].

[18] "Spec 5851 SunGen XLPE, Photovoltaic Wire, 2000 V, UL Type PV or 1000 V, CSA RPVU90, Single Conductor, Copper." [Online]. Available: http://dtsheet.com/doc/1724396/spec-5851-sungen-xlpe--photovoltaic-wire--2000-v--ul-type... [Accessed: 02-Oct-2019].

[19] N. K. T. Jayakumar *et al.*, "Postprocessing for Improved Accuracy and Resolution of Spread Spectrum Time-Domain Reflectometry," *IEEE Sens. Lett.*, vol. 3, no. 6, pp. 1–4, Jun. 2019.

Ayobami S. Edun received the B.Eng. degree in electrical and electronics engineering from Federal University of Technology, Akure, Nigeria in 2014. He received the M.S. degree in electrical and computer engineering from University of Florida, Gainesville, FL, USA in 2019. He is currently working towards the PhD degree in Electrical and Computer Engineering at the University of Florida, Gainesville, FL, USA. He currently works as a Research Assistant at the SmartDATA Lab, University of Florida, Gainesville, FL. He has been working with spread spectrum time domain reflectometry (SSTDR) in being able to detect, localize, and characterize faults within solar panel system.

Naveen Kumar T. Jayakumar was born in Bangalore, India, in 1992. He received the B.S. degree from Visvesvaraya Technological University, Karnataka, India, in 2014 and the M.S. degree in electrical engineering from University of, Utah, Salt Lake City, UT, USA in 2019.

From 2014 to 2016, he worked as an embedded software engineer at Robert Bosch, Bangalore, India. After that, he worked as a Research Assistant with the Department of Electrical Engineering at the University of Utah from August 2017 to December 2018. His research interests include antenna design for wireless wearables, RFIC design, SSTDR for fault detection in photovoltaic panels and microwave engineering.

Samuel R. Kingston was born in Salt Lake City, Utah, UT, USA in 1991. He received the A.S. degree in business from Salt Lake Community College, Salt Lake City, in 2011. He received a B.S. degree in electrical & computer engineering from the University of Utah, Salt Lake City, UT, in 2016 and is currently working on a Ph. D from the University of Utah, Salt Lake City, UT.

From 2017 to current, he has been a Research Assistant with the University of Utah lab working in the algorithms group. He has been working with spread spectrum time domain reflectometry (SSTDR) in being able to detect, localize, and characterize faults within solar panel system. To date, he has written a conference paper for nondestructive health monitoring. He is currently working on several journal papers, where each one will be a building block in achieving the overall research team goal. His research interests are in signal processing used for health monitoring, renewable energy alternatives, and creating successful startups from conceptual ideas. In 2016, his senior project team received an award for best clinic project where he worked with L3 communications to develop a way to detect low probability of intercept (LPI) RADAR signals.

Cynthia M. Furse (M'85–SM'99–F'08) is Professor of Electrical and Computer Engineering at the University of Utah. Dr. Furse received her B.S. in electrical engineering with a mathematics minor in 1985, M.S. degree in electrical engineering in 1988, and her Ph.D. in electrical engineering from the University of Utah in 1994.

She has applied her expertise in electromagnetics to sensing and communication in complex lossy scattering media such as the human body, geophysical prospecting, ionospheric plasma, and aircraft wiring networks. She has taught electromagnetics, wireless communication, computational electromagnetics, microwave engineering, antenna design, and introductory electrical engineering and has been a leader in the development of the flipped classroom.

Dr. Furse is a Fellow of the IEEE and the National Academy of Inventors. She is a past AdCom member for the IEEE AP society and past chair of the IEEE AP Education Committee. She has received numerous teaching and research awards including the 2009 IEEE Harriett B. Rigas Medal for Excellence in Teaching. She is a founder of LiveWire Innovation, Inc., a spin-off company commercializing devices to locate intermittent faults on live wires.

Michael A. Scarpulla (M'05-SM'14) earned the Sc.B. degree from Brown University in 2000 and the PhD from UC Berkeley in 2006, both in Materials Science and Engineering. His PhD work focused on laser processing of ion implanted compound semiconductors, carrier mediated ferromagnetism, and multiband semiconductors. From 2006-2008 he was a postdoctoral scholar at UC Santa Barbara working on epitaxial integration of rare-earth pnictides with III-V semiconductors using MBE. Since joining the ECE and MSE faculties at University of Utah in 2008, he has worked in light trapping for photovoltaics, materials processing and characterization of chalcogenide thin film photovoltaics, reflectometry in photovoltaic systems, and defects in wide-bandgap semiconductors. His hobbies include skiing, climbing, and other mountain adventures.

Joel B. Harley (S'05-M'14) received his B.S. degree in Electrical Engineering from Tufts University in Medford, MA, USA. He received his M.S. and Ph.D. degrees in Electrical and Computer Engineering from Carnegie Mellon University in Pittsburgh, PA, USA in 2011 and 2014, respectively.

In 2018, he joined the University of Florida, where he is currently an assistant professor in the Department of Electrical and Computer Engineering. Previously, he was an assistant professor in the Department of Electrical and Computer Engineering at the University of Utah. His research interests include integrating novel signal processing, machine learning, and data science methods for the analysis of waves and time-series data.

Dr. Harley's awards and honors include an Air Force Summer Faculty Fellowship Award, Air Force Young Investigator Award, the Carnegie Mellon University A. G. Jordan Award for academic excellence and service, and a National Science Foundation Graduate Research Fellowship. He has published more than 60~technical journal and conference papers, including three that were chosen as best student papers. He is currently the student representative advisor for the IEEE Ultrasonic, Ferroelectrics, and Frequency Control Society, member of the IEEE Signal Processing Society, and a member of the Acoustical Society of America.